nature chemistry

ARTICLES

https://doi.org/10.1038/s41557-018-0015-x

O_2–O_2 and O_2–N_2 collision-induced absorption mechanisms unravelled

Tijs Karman[1], Mark A. J. Koenis[2], Agniva Banerjee[1], David H. Parker[1], Iouli E. Gordon[3], Ad van der Avoird[1], Wim J. van der Zande[1] and Gerrit C. Groenenboom[1*]

Collision-induced absorption is the phenomenon in which interactions between colliding molecules lead to absorption of light, even for transitions that are forbidden for the isolated molecules. Collision-induced absorption contributes to the atmospheric heat balance and is important for the electronic excitations of O_2 that are used for remote sensing. Here, we present a theoretical study of five vibronic transitions in O_2–O_2 and O_2–N_2, using analytical models and numerical quantum scattering calculations. We unambiguously identify the underlying absorption mechanism, which is shown to depend explicitly on the collision partner—contrary to textbook knowledge. This explains experimentally observed qualitative differences between O_2–O_2 and O_2–N_2 collisions in the overall intensity, line shape and vibrational dependence of the absorption spectrum. It is shown that these results can be used to discriminate between conflicting experimental data and even to identify unphysical results, thus impacting future experimental studies and atmospheric applications.

The selection rules that govern atomic and molecular spectroscopy are related to symmetry restrictions, which imply vanishing transition strength to a certain degree of approximation. Symmetry is broken by collisions with other molecules in the gas phase, which lifts the selection rules and induces otherwise forbidden electric dipole transitions, leading to so-called collision-induced absorption[1]. Collision-induced absorption was discovered by Welsh and co-workers for forbidden vibrational transitions in compressed O_2 and N_2 gases[2]. More recent measurements of collision-induced absorption typically use cavity ring-down spectroscopy to observe the weak collision-induced signal by achieving long path lengths[3–11], rather than high pressures[12,13]. Roto-translational collision-induced absorption is important for the atmospheric heat balance[14], and electronic transitions in O_2, such as the A-band $X^3\Sigma_g^- \rightarrow b^1\Sigma_g^+(v'=0)$ transition[15–19] and the 1.27 μm band $X^3\Sigma_g^- \rightarrow a^1\Delta_g(v'=0)$ transition[20], have gained significant attention as they are observable in Earth's atmosphere and used in remote sensing calibration. Absorption for these transitions is due to spin–orbit-allowed magnetic dipole lines, but collision-induced absorption also contributes significantly. Oxygen collision-induced absorption has also been put forward as a biomarker to be observed in exo-planetary atmospheres[21], where the quadratic pressure dependence can be used to probe the atmospheric distribution, in addition to the column density.

The theoretical treatment of collision-induced absorption is well established for rotation–translation and vibrational transitions[1], and it is well known that such spectra are typically dominated by quadrupole induced dipole moments. Electronic transitions have been studied theoretically for forbidden $^1S \rightarrow {}^1D$ transitions in atom–atom collisions[22,23], and the mechanism is again quadrupole induction. By contrast, for spin-forbidden electronic transitions, the mechanism cannot be only quadrupole induction, as this interaction does not lift the spin selection rule. Mechanisms for breaking spin symmetry have been suggested[24–30], but not identified in absorption spectra, despite extensive experimental studies. The most extensively studied spin-forbidden transitions are electronic transitions of molecular oxygen. In 1885, Janssen first observed the oxygen A-band in dense gases[31,32], long before the process was identified as collision-induced absorption[33]. More recently, atmospheric applications have motivated numerous experimental studies, which observe both monomer absorption lines and collision-induced absorption[3–13,34–36]. A line shape theory does not yet exist, neither for spin-forbidden transitions nor for collision-induced molecular electronic transitions in general.

Here, we theoretically study the $X^3\Sigma_g^- \rightarrow a^1\Delta_g$ and $X^3\Sigma_g^- \rightarrow b^1\Sigma_g^+$ transitions of molecular oxygen in O_2–O_2 and O_2–N_2 collisions. These transitions are monomer-forbidden by both spin ($S=1 \nrightarrow 0$) and spatial ($g \nrightarrow g$) selection rules. The most influential monograph on collision-induced absorption states the following about these specific transitions[1]: 'For collisional induction of these bands a foreign molecule is more or less as expedient as an O_2 molecule. The specific properties of the collisional partner hardly matter as long as it is not absent.' In this Article, however, we show that the underlying absorption mechanism depends on the specific properties of the collisional partner and that this leads to qualitative differences in the intensity, line shape and vibrational dependence of the absorption spectra. To this end, we present the first theoretical line shape study of electronic transitions in molecular collision-induced absorption.

In a bimolecular collision, the symmetry of the system is broken and the spatial selection rules are relaxed. However, this does not lift the selection rule on spin multiplicity. Three different mechanisms have been proposed to break the spin symmetry:

The first mechanism, the spin–orbit mechanism, takes into account the intramolecular spin–orbit coupling between the $X^3\Sigma_g^-, \Omega=0^+$ and $b^1\Sigma_g^+$ states of O_2, which mixes these states with coefficient $C=0.0134i$. This mixing of singlet and triplet electronic states lifts the spin selection rules[25–28]. This leads to spin–orbit-allowed magnetic dipole and electric quadrupole transition moments and the associated monomer absorption lines. In a collision complex, the breaking of spin symmetry leads to transition dipole moments, through quadrupole induction. This dipole moment is long ranged and varies with R^{-4}, where R is the intermolecular distance.

[1]Institute for Molecules and Materials, Radboud University, Nijmegen, the Netherlands. [2]Van 't Hoff Institute for Molecular Sciences, University of Amsterdam, Amsterdam, the Netherlands. [3]Harvard-Smithsonian Center for Astrophysics, Cambridge, MA, USA. *e-mail: gerritg@theochem.ru.nl

The second mechanism, the exchange mechanism, applies only to paramagnetic collision partners. In this case, the total electron spin of the collision complex is conserved, making the transition formally allowed, even though the O_2 monomer spin changes from triplet to singlet. For example, for the O_2–O_2 collisions considered here,

$$O_2(X^3\Sigma_g^-) + O_2(X^3\Sigma_g^-) + h\nu \rightarrow O_2(a^1\Delta_g / b^1\Sigma_g^+) + O_2(X^3\Sigma_g^-).$$

The final state is a total spin triplet state of the complex, whereas the initial state has two triplet molecules, which can couple to overall singlet, triplet and quintet spin states. For transitions between triplet states, the formal spin restriction has been lifted. Non-zero intensity for this process is due to the exchange interaction between paramagnetic collision partners[24], and the induced dipole moment decays exponentially with the intermolecular distance, as $\exp(-\gamma R)$.

The heavy-atom effect is a possible third mechanism, where interaction with a heavier element enhances relativistic effects such as spin–orbit coupling[25,29,30]. This mechanism is not considered here because it is less relevant for collisions with light atmospherically abundant collision partners such as N_2 and O_2.

Results

Theory. We calculated bimolecular collision-induced absorption spectra for the $X^3\Sigma_g^- \rightarrow a^1\Delta_g$ and $b^1\Sigma_g^+$ transitions in O_2–O_2 and O_2–N_2, for both the exchange and spin–orbit mechanisms. Such line shape calculations, which have previously been performed only for roto-translational and vibrational (RT&V) transitions, obtain the absorption spectrum from dipole coupling between the scattering wavefunctions that describe the colliding molecules, which are calculated using coupled-channels theory[1]. These calculations require the electronic energy and transition dipole moments for the electronic ground and six electronically excited states of the complex as a function of the nuclear coordinates. We calculated these four-dimensional potential energy and exchange-induced transition dipole moment surfaces using ab initio electronic structure methods[37]. The essential innovation that enabled these calculations was diabatization of these surfaces, which includes non-adiabatic couplings beyond the Born–Oppenheimer approximation. To this end, we used a novel multiple-property-based diabatization algorithm, which has been developed as a part of this project[38]. This treatment is crucial due to the occurrence of seams of conical intersections at which derivative couplings are divergent. The issue of diabatization is not encountered for RT&V dipole surfaces, which involve only the electronic ground state. Similarly unfamiliar from RT&V transitions is the first-principles computation of intermolecular exchange-induced properties, which is virtually unexplored[39], and is shown here to be challenging. For the spin–orbit mechanism, we employ the long-range model that we developed in ref. [40], which involves the spin–orbit-induced transition quadrupole moment of O_2. In this work, scattering wavefunctions are calculated in the approximation of an isotropic interaction between the colliding molecules. This allows decoupling of the radial and angular degrees of freedom and the latter to be treated analytically, thus significantly reducing the computational effort. The isotropic approximation applies only to the interaction potential, whereas the full anisotropic transition dipole surface is used. This approximation is commonly used in line shape calculations for RT&V bands, and we have extended this theory to electronic transitions[40]. We also present corrections to this approximation from classical statistical mechanics, using the full anisotropic interaction. Numerical results suggest that the effect of anisotropy is more pronounced for electronic transitions than for RT&V bands. A more detailed discussion of all the calculations is provided in the Supplementary Information and supporting references[37,38,40].

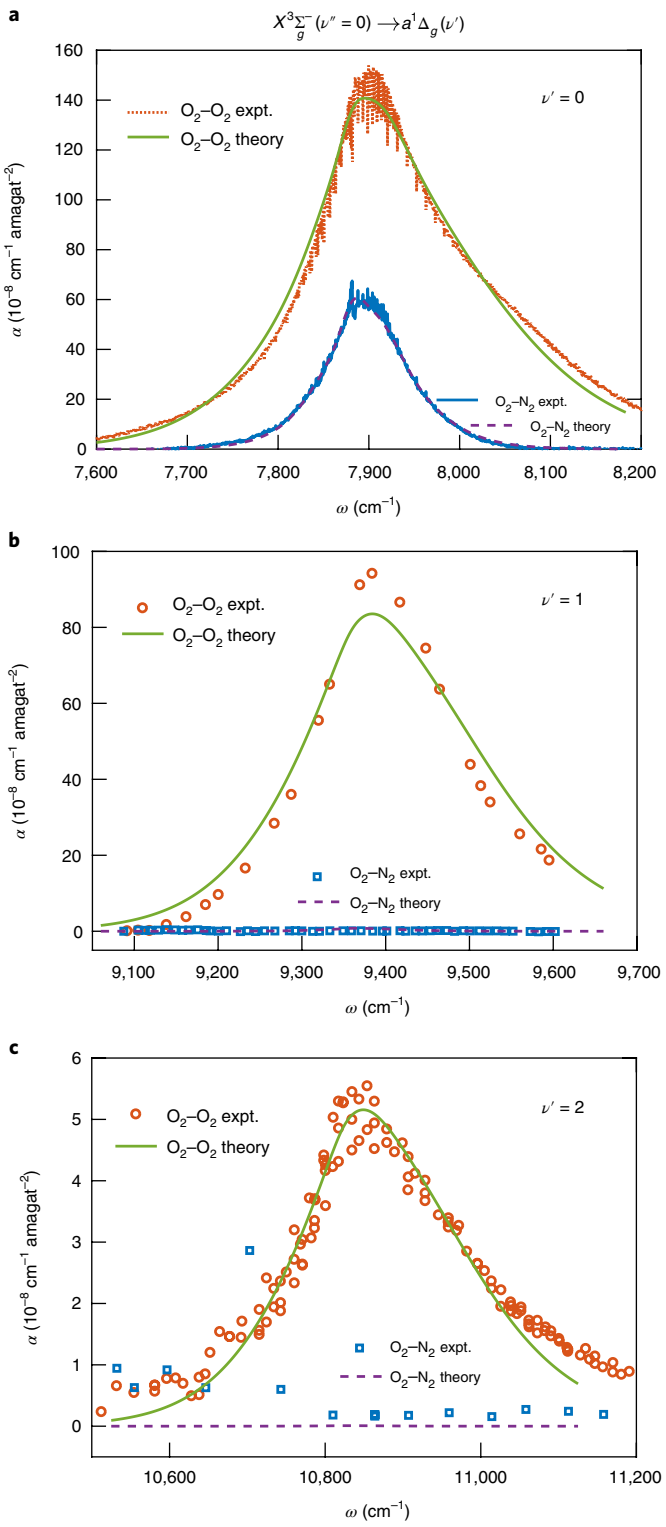

Fig. 1 | Experimental and theoretical collision-induced absorption spectra for the $X^3\Sigma_g^-(v''=0) \rightarrow a^1\Delta_g(v')$ bands of O_2–O_2 and O_2–N_2. a–c, Spectra corresponding to $v'=0$ (**a**), 1 (**b**) and 2 (**c**), where experimental data are taken from ref. [4], this work and ref. [9], respectively. The absorption coefficient, α, is normalized to the square of the number density, which is measured in amagat, the number density of an ideal gas at 1 atm and 0 °C. Absorption by O_2–O_2 is more intense and broader in frequency than for O_2–N_2. Vibrational transitions $v'>0$ are observed for O_2–O_2 but not for O_2–N_2. The intensity for the spin–orbit mechanism follows the predicted scaling with Franck–Condon factors, whereas the suppression is evidently less strong for the exchange contribution, which only contributes for O_2–O_2.

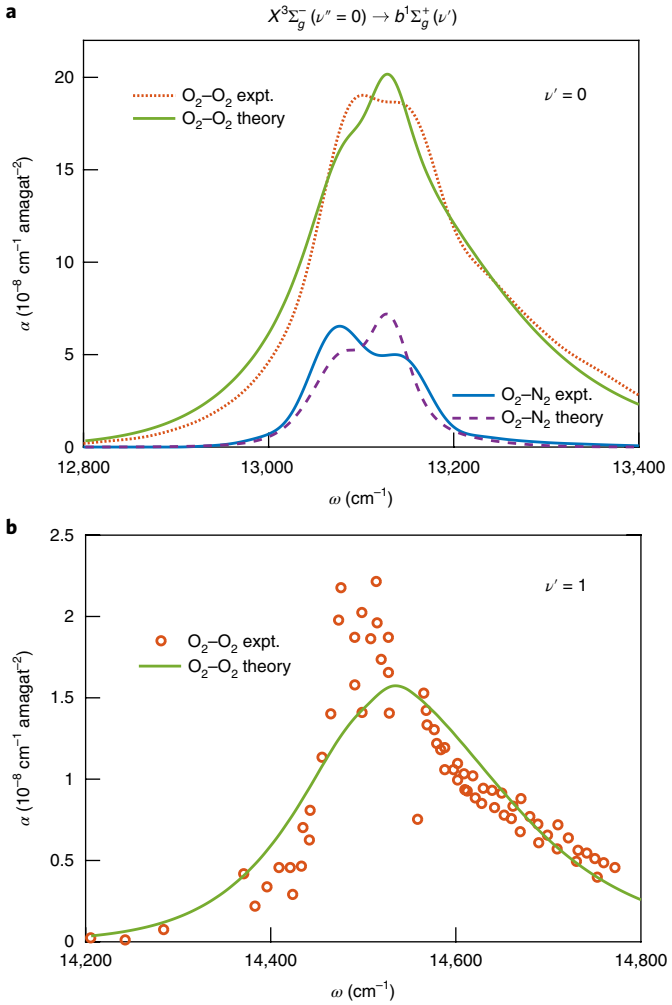

Fig. 2 | Experimental and theoretical collision-induced absorption spectra for the $X^3\Sigma_g^-(v''=0) \rightarrow b^1\Sigma_g^+(v')$ bands of O_2–O_2 and O_2–N_2. a,b, Spectra corresponding to $v'=0$ (**a**) and 1 (**b**), where experimental data are taken from ref. [7] and ref. [12], respectively. Absorption by O_2–O_2 is more intense and broader in frequency than for O_2–N_2.

Figures 1 and 2 present collision-induced absorption spectra for $X^3\Sigma_g^- \rightarrow a^1\Delta_g$ and $X^3\Sigma_g^- \rightarrow b^1\Sigma_g^+$ transitions, respectively. The $a^1\Delta_g(v'=1)$ band was measured in this work using cavity ring-down spectroscopy, similar to the method used in ref. [6], and is described in more detail in Supplementary Section 6. Experimental data for the $a^1\Delta_g(v'=0, 2)$ and $b^1\Sigma_g^+(v'=0, 1)$ bands are taken from refs [4,7,9,12], and are the HITRAN recommended data wherever multiple experiments exist[41,42]. The theoretical line shapes match the experimental results well. However, to also achieve agreement for the intensities, the theory was scaled by the factors shown in Table 1. The scaling factors for the exchange mechanism, c_{Exch}, seem large, but, as shown below, they are within the uncertainty of the calculated intensity (which is due to the large uncertainty of the dipole surfaces for this mechanism). The predicted line shapes are unaffected by this uncertainty. For the spin–orbit mechanism, where the dipole surface is known more accurately, the anisotropy-corrected scaling factors are closer to unity.

Intensity. From the absorption spectra in Figs. 1 and 2, qualitative differences between O_2–O_2 and O_2–N_2 collision-induced absorption become apparent. The O_2–O_2 contributions are typically more intense, significantly broader in frequency, and decay less rapidly

Table 1 | Scale factors for theoretical line shapes fit to experimental data

Transition	$c_{\mathrm{Exch}}^{O_2-O_2}$	$c_{\mathrm{SO}}^{O_2-O_2}$	$c_{\mathrm{SO}}^{O_2-N_2}$
$X^3\Sigma_g^- \rightarrow a^1\Delta_g(v'=0)$	4.48	1.10	1.68
$X^3\Sigma_g^- \rightarrow a^1\Delta_g(v'=1)$	2.90		
$X^3\Sigma_g^- \rightarrow a^1\Delta_g(v'=2)$	0.15		
$X^3\Sigma_g^- \rightarrow b^1\Sigma_g^+(v'=0)$	6.41	0.66	0.71
$X^3\Sigma_g^- \rightarrow b^1\Sigma_g^+(v'=1)$	0.63		

Scaling factors are shown for both the exchange (Exch) and spin-orbit (SO) mechanisms. Classical statistical mechanical corrections for anisotropic interactions have been included (Supplementary Section 3).

with increasing vibrational excitation v'. The difference in line shape is seen even more clearly on a logarithmic scale (Fig. 5). The observed difference in intensity can be understood as the O_2–N_2 intensity is solely due to the spin–orbit mechanism, whereas the O_2–O_2 intensity is dominated by the additional exchange mechanism, and the contribution of the spin–orbit mechanism is observable only near the line centre.

Line shape. The difference in line shape can also be understood from these mechanisms and the correspondingly different geometry dependence of the transition dipole moment. The dipole moment of the spin–orbit mechanism, which is the only contribution for O_2–N_2, results from long-range spin–orbit-induced quadrupole induction and depends on the intermolecular distance, R, as R^{-4}. This drives electronic transitions at comparatively long length scales—and therefore long timescales—which leads to a relatively narrow absorption feature. By contrast, the dipole moment of the exchange mechanism, which dominates for O_2–O_2, decays exponentially with intermolecular distance. This induces electronic transitions at very short length and timescales, leading to a much broader absorption spectrum.

To rigorously demonstrate the relation between line shape and absorption mechanism, we considered an analytical model for the translational profile, VG, which determines the absorption line shape (Supplementary Section 1e). This model accounts for hard-sphere scattering (with radius a) at a single energy $E=k_BT$ and dipole functions proportional to $\exp(-\gamma R)$ and R^{-4}, respectively. This yields for the exchange (Exch) and spin-orbit (SO) mechanisms:

$$VG_{\mathrm{Exch}}(\omega) = \frac{\gamma^2 k k'}{\{(\gamma^2+k^2)^2 + 2(\gamma^2-k^2)k'^2 + k'^4\}^2}$$
$$VG_{\mathrm{SO}}(\omega) = \frac{1}{kk'}\left[G_{1,3}^{3,1}\left(\frac{a^2}{4}[k-k']^2 \;\middle|\; \begin{matrix} 0 \\ 0 \end{matrix} \; \begin{matrix} \frac{3}{2} & 2 \end{matrix}\right)\right]^2 \qquad (2)$$

where $G_{1,3}^{3,1}$ denotes a Meijer G function[43] and the initial- and final-state wavenumbers are given by $k=\sqrt{2\mu k_BT}$ and $k'=\sqrt{2\mu(k_BT+\hbar\omega)}$, respectively. These profiles are compared to the results of the full calculations in Fig. 3, using realistic parameters $a=7a_0$ and $\gamma=3a_0^{-1}$. The analytical model reproduces the typical translational profiles, supporting the length-scale argument presented above.

Vibrational dependence. The differences in v' dependence, seen in Figs. 1 and 2, are explained by the vibrational dependence of the transition dipole moments. In the spin–orbit mechanism, the only contribution for O_2–N_2, the dipole moment is proportional to the spin–orbit-induced transition quadrupole moment of O_2.

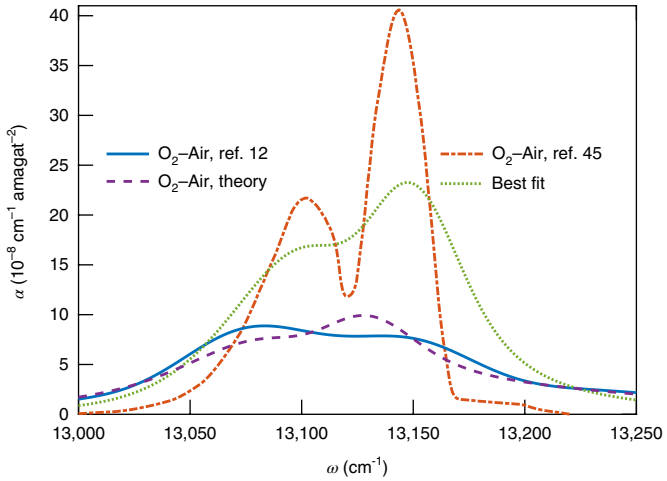

Fig. 3 | Collision-induced absorption spectra for the $X^3\Sigma_g^-(v''=0) \rightarrow b^1\Sigma_g^+(v'=0)$ band in air, normalized to the product of O_2 and air number densities. The experimental spectra of ref. [12] and of the more recent ref. [45] differ significantly. The line shape of ref. [45] is even narrower than the theoretical line shape for the spin–orbit mechanism, which is indicated as the best fit. A narrower line shape requires a dipole moment of longer range than R^{-4}, which is unphysical.

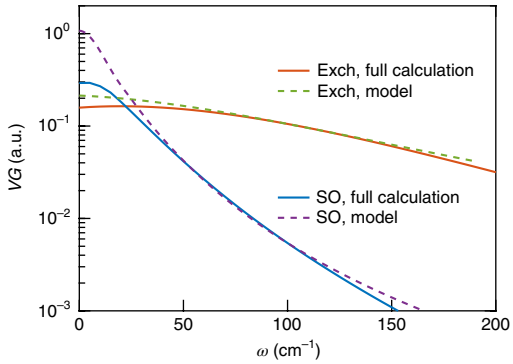

Fig. 4 | Translational profiles for the $X^3\Sigma_g^- \rightarrow a^1\Delta_g$ transition for both exchange and spin–orbit mechanisms. Results of the full line shape calculation are compared to the results of the analytical hard-sphere model (discussed in detail in Supplementary Section 1e) for both the exchange (Exch) and spin-orbit (SO) mechanisms. The analytical model describes the decay in the wing well, indicating that the line shape is determined by the range of the induced dipole moment.

This transition quadrupole moment is only weakly dependent on the O_2 bond length, and so the intensities of transitions to $v'>0$ are suppressed following the Franck–Condon factors. For the bands studied here, the Franck–Condon factors are small, ranging from 1×10^{-4} to 7×10^{-2} (ref. [44]). Therefore, the $v'>0$ transitions are heavily suppressed for O_2–N_2 and are not observed. For the exchange mechanism, which is dominant for O_2–O_2, the vibrational dependence is evidently much stronger, as $v'>0$ bands are suppressed by much less than the Franck–Condon factor. This can be understood as the transition dipole moment for this mechanism depends on the nuclear geometry—including vibrational coordinates—with exponential sensitivity. This is shown by exploratory electronic structure calculations, presented in Supplementary Section 2, which yield a vibrational dependence that is in qualitative agreement with the scaling factors in Table 1.

Analysis of experimental spectra. The insight into the absorption mechanism and resulting spectral signatures developed in the previous sections can be used to analyse conflicting experimental line shapes. This is illustrated in Fig. 4, which shows collision-induced absorption spectra for the oxygen A-band $X^3\Sigma_g^- \rightarrow b^1\Sigma_g^+(v'=0)$ transition in air, that is, 21% O_2 and 79% N_2. The experimental results in ref. [12] and the theoretical spectrum correspond to those shown in Fig. 2a. Figure 4 also contains data from the recent multispectrum fitting study of ref. [45]. The experimental spectra differ significantly, and the line shape of ref. [45] is narrower and more structured. The collision-induced line shape of ref. [45] is even narrower than the narrowest theoretical result, corresponding to the R^{-4} spin–orbit mechanism, indicated as 'Best fit' in Fig. 4. This implies that the line shape of ref. [45] can only be reproduced by assuming a transition dipole moment that has an even longer range than R^{-4}; that is, the line shape is unphysically narrow.

By contrast, the widths of the spectra of ref. [12] match the theoretical predictions well, for both O_2–O_2 and O_2–N_2. However, deviations between theory and the experiment of ref. [12] are observed in the structure near the band centre, which is also visible in Fig. 2a. In the theoretical spectra, the high-frequency wing is always more intense than the low-frequency wing due to the detailed balance relation developed in Supplementary Section 1g, which the experimental spectrum is seen to violate. This approximate detailed balance relation assumes a weak dependence of the potential on the electronic state.

In the experiments compared above, the total absorption is measured directly, and the experimental collision-induced absorption spectra are obtained by subtracting a line-by-line model of the monomer absorption. This analysis can lead to a dependence of the extracted collision-induced absorption on line-by-line parameters such as line mixing[12,45]. Analysis of experimental spectra is particularly difficult for the A-band, where the differences between experiment and theory are largest, because collision-induced absorption is weakest and magnetic dipole lines are strongest for this transition. Thus, the marked deviations from theory do not disqualify either measurement; rather they expose the limitations of the line-by-line absorption models employed and issues with parameter correlation. In this context, the presented line shape theory is a useful constraint on experimental data, which could improve fitting and extrapolation of measured absorption and hence further improve the accuracy of atmospheric measurements.

Discussion

Finally, we estimated the uncertainty of our calculations, which had two sources. First, the scattering dynamics is treated approximately, using isotropic interaction potentials. Second, the used potential energy and transition dipole moment surfaces are inexact.

Including interaction anisotropy in quantum-mechanical line shape calculations is prohibitively computer intensive[46] and not attempted here. Yet, we can provide estimates of the effects of interaction anisotropy from a classical statistical mechanical theory, as used in ref. [47] and discussed in more detail in Supplementary Section 3. We note that quantum corrections to this formalism are available[48], but have not been included. In this theory, the integrated intensity—but not the line shape—is calculated from a thermal average of the squared transition dipole moment. These integrals over the dimer configuration space can be performed using either isotropic or anisotropic potentials, and the ratio of these results provides an estimate of the effect of anisotropy on the intensity. We find that anisotropic interactions enhance the intensity by a factor of 2 to 4 for the bands considered here, indicating that full inclusion of anisotropy is necessary to reproduce the experiment. We note that, when this procedure is applied to the roto-translational band of N_2–N_2, we find 20% enhancement of the intensity at $T=78$ K, but essentially no effect at room temperature, in agreement with the

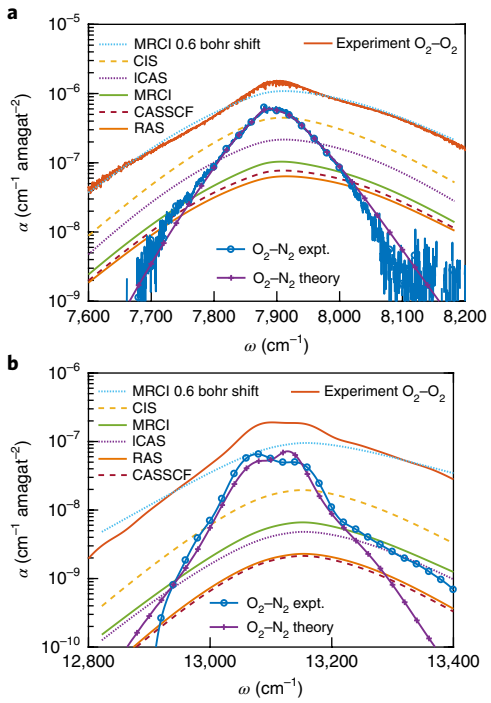

Fig. 5 | Collision-induced absorption spectra for the $X^3\Sigma_g^- \rightarrow a^1\Delta_g$ and $b^1\Sigma_g^+$ transitions in O_2–O_2 and experimental results. a,**b**, Experimental spectra in panels **a** and **b** are from ref. [4] and ref. [12], respectively. Theoretical spectra based on the exchange mechanism are calculated using various dipole moment surfaces, as indicated in the legend in the figure. These predictions differ by an order of magnitude in intensity but predict identical line shapes, which differ substantially from the more narrow O_2–N_2 results included for comparison.

full line shape calculations of ref. [46]. To further investigate the effect of anisotropy, we performed line shape calculations using a radially shifted isotropic potential. As shown in Fig. 5, agreement of the total intensity requires a shift of 0.6–0.7a_0, which is small compared to the neglected anisotropy of the classical turning point of the potential, which varies between 7.5a_0 for collinear geometries and 5.4a_0 for parallel orientations. These results suggest that the effect of anisotropy may be more substantial for the electronic transitions studied here than for their well-studied roto-translational counterparts.

The accuracy of our calculations was further affected by the accuracy of the transition dipole surfaces. To give an estimate of the associated uncertainty, we calculated the absorption spectra with **a** number of dipole surfaces, as shown in Fig. 5. This includes the MRCI and CASSCF dipole surfaces of ref. [37] and additional surfaces denoted CIS, *l*CAS and RAS, calculated in the present work. A more detailed description is provided in Supplementary Section 4. The methods used to calculate these transition dipole moment surfaces differ only in the treatment of electron correlation, and the observed differences represent a rather surprising result. Dipole moments for allowed transitions are typically accurately calculated at low levels of theory, as they are of one-electron character and hence insensitive to hard-to-treat effects such as electron correlation. The transitions studied here are induced by the intermolecular exchange interaction and are not simple one-electron transitions, so the effects of electron correlation are surprisingly pronounced. The predicted intensities differ by factors up to 10, so the scaling factors of Table 1 are within the 'theoretical error bars'. More importantly, the predicted line shape is unaffected by this uncertainty, which motivates the analysis in terms of theoretical line shapes but not intensities, presented in this Article. This can be understood from analysis of the line shape, presented in Supplementary Section 1c. The line shape is sensitive to the exp($-\gamma R$) decay with intermolecular separation R, but is affected less by the intensity and anisotropy of the dipole surface, which remain uncertain.

Conclusions

In conclusion, we have presented the first line shape calculations for spin-forbidden electronic transitions in bimolecular collisions, which permit the unambiguous identification of the absorption mechanism for the $X^3\Sigma_g^- \rightarrow a^1\Delta_g(v'=0,1,2)$ and $b^1\Sigma_g^+(v'=0,1)$ bands in O_2–O_2 and O_2–N_2. The absorption mechanism is shown to depend on the specific properties of the collision partner, which contradicts the conventional wisdom in the field[1]. Only if the perturbing molecule has non-zero electron spin does an intermolecular-exchange mechanism contributes to the absorption, in addition to a spin–orbit-based mechanism. As a result, the O_2–O_2 absorption spectra—when compared to O_2–N_2—are more intense, broader in frequency and decay less rapidly with v', violating the v' dependence expected from Franck–Condon factors. These spectral signatures of the absorption mechanism are reproduced by our ab initio calculations and are explained by the difference in range—R^{-4} versus exp($-\gamma R$)—of the induced transition dipole moment for the two underlying absorption mechanisms. The radial dependence of these mechanisms is not specific to the studied systems, so our conclusions are more generally applicable. The presented results impact experimental studies, where analysis of the spectral line shape allows the relative contribution of the underlying absorption mechanisms to be extracted and even to identify unphysical results, as illustrated for conflicting experimental data for the oxygen A-band[12,45]. Furthermore, this study motivates the development of electronic structure methods to calculate converged exchange-induced transition dipole moments, which presently have surprisingly large theoretical error bars due to the sensitivity to electron correlation.

Data availability. All measured and calculated absorption spectra are available in the Supplementary Information.

Received: 18 September 2017; Accepted: 23 January 2018;
Published online: 09 April 2018

References

1. Frommhold, L. *Collision-Induced Absorption in Gases* (Cambridge Univ. Press, Cambridge, 1994).
2. Crawford, M. F., Welsh, H. L. & Locke, J. L. Infra-red absorption of oxygen and nitrogen induced by intermolecular forces. *Phys. Rev.* **75**, 1607–1607 (1949).
3. Smith, K. M. & Newnham, D. A. Near-infrared absorption cross sections and integrated absorption intensities of molecular oxygen (O_2, O_2–O_2, and O_2–N_2). *J. Geophys. Res. Atmos.* **105**, 7383–7396 (2000).
4. Maté, B., Lugez, C., Fraser, G. T. & Lafferty, W. J. Absolute intensities for the O_2 1.27 μm continuum absorption. *J. Geophys. Res. Atmos.* **104**, 30585–30590 (1999).
5. Long, D. A., Robichaud, D. J. & Hodges, J. T. Frequency-stabilized cavity ring-down spectroscopy measurements of line mixing and collision-induced absorption in the O_2 A-band. *J. Chem. Phys.* **137**, 014307 (2012).
6. Spiering, F. R. et al. Line mixing and collision induced absorption in the oxygen A-band using cavity ring-down spectroscopy. *J. Chem. Phys.* **133**, 114305 (2010).
7. Spiering, F. R., Kiseleva, M. B., Filippov, N. N., van Kesteren, L. & van der Zande, W. J. Collision-induced absorption in the O_2 B-band region near 670 nm. *Phys. Chem. Chem. Phys.* **13**, 9616–9621 (2011).
8. Spiering, F. R. et al. The effect of collisions with nitrogen on absorption by oxygen in the A-band using cavity ring-down spectroscopy. *Mol. Phys.* **109**, 535–542 (2011).
9. Spiering, F. R. & van der Zande, W. J. Collision induced absorption in the $a^1\Delta(v=2) \leftarrow X^3\Sigma_g^-(v=0)$ band of molecular oxygen. *Phys. Chem. Chem. Phys.* **14**, 9923–9928 (2012).
10. Sneep, M. & Ubachs, W. Cavity ring-down measurement of the O_2–O_2 collision-induced absorption resonance at 477 nm at sub-atmospheric pressures. *J. Quant. Spectrosc. Radiat. Transf.* **78**, 171–178 (2003).

11. Sneep, M. & Ubachs, W. in *Weakly Interacting Molecular Pairs: Unconventional Absorbers of Radiation in the Atmosphere* Vol. 27 (eds Camy-Peret, C. & Vigasin, A.) 203–211 (NATO Science Series: IV: Earth and Environmental Sciences, Springer, 2003).
12. Tran, H., Boulet, C. & Hartmann, J.-M. Line mixing and collision-induced absorption by oxygen in the A-band: laboratory measurements, model, and tools for atmospheric spectra computations. *J. Geophys. Res.* **111**, D15210 (2006).
13. Vangvichith, M., Tran, H. & Hartmann, J.-M. Line-mixing and collision induced absorption for O_2CO_2 mixtures in the oxygen A-band region. *J. Quant. Spectrosc. Radiat. Transf.* **110**, 2212–2216 (2009).
14. Höpfner, M., Milz, M., Buehler, S., Orphal, J. & Stiller, G. The natural greenhouse effect of atmospheric oxygen (O_2) and nitrogen (N_2). *Geophys. Res. Lett.* **39**, L10706 (2012).
15. Eldering, A. et al. High precision atmospheric CO_2 measurements from space: the design and implementation of OCO-2. In *Proc. 2012 IEEE Aerospace Conference* 1–10 (IEEE, 2012).
16. Miller, C. E. et al. Precision requirements for space-based data. *J. Geophys. Res. Atmos.* **112**, D10314 (2007).
17. Kuang, Z., Margolis, J. S., Toon, G. C., Crisp, D. & Yung, Y. L. Spaceborne measurements of atmospheric CO_2 by high-resolution nir spectrometry of reflected sunlight: an introductory study. *Geophys. Res. Lett.* **29**, 1716 (2002).
18. O'Brien, D. M., Mitchell, R. M., English, S. A. & Costa, G. A. D. Airborne measurements of air mass from O_2 A-band absorption spectra. *J. Atmos. Ocean. Technol.* **15**, 1272–1286 (1998).
19. Diedenhoven, Bv, Hasekamp, O. P. & Aben, I. Surface pressure retrieval from SCIAMACHY measurements in the O_2 A-band: validation of the measurements and sensitivity on aerosols. *Atmos. Chem. Phys.* **5**, 2109–2120 (2005).
20. Wunch, D. et al. The total carbon column observing network. *Philos. Trans. R. Soc. A* **369**, 2087–2112 (2011).
21. Misra, A., Meadows, V., Claire, M. & Crisp, D. Using dimers to measure biosignatures and atmospheric pressure for terrestrial exoplanets. *Astrobiology* **14**, 67–86 (2014).
22. Gallagher, A. & Holstein, T. Collision-induced absorption in atomic electronic transitions. *Phys. Rev. A.* **16**, 2413 (1977).
23. Julienne, P. S. Non-adiabatic theory of collision-broadened atomic line profiles. *Phys. Rev. A.* **26**, 3299–3317 (1982).
24. Robinson, G. W. Intensity enhancement of forbidden electronic transitions by weak intermolecular interactions. *J. Chem. Phys.* **46**, 572 (1967).
25. Minaev, B. Intensities of spin-forbidden transitions in molecular oxygen and selective heavy-atom effects. *Int. J. Quantum Chem.* **17**, 367–374 (1980).
26. Minaev, B. F. & Ågren, H. Collision-induced $b^1\text{-}\ ^1\Sigma_g^-$ $a^1\Delta_g$, $b^1\Sigma_g^+$ -$X^3\Sigma_g^-$ and $a^1\Delta_g$-$X^3\Sigma_g^-$ transition probabilities in molecular oxygen. *J. Chem. Soc. Faraday Trans.* **93**, 2231–2239 (1997).
27. Minaev, B. F. & Kobzev, G. I. Response calculations of electronic and vibrational transitions in molecular oxygen induced by interaction with noble gases. *Spectrochim. Acta A* **59**, 3387–3410 (2003).
28. Minaev, B. F. Electronic mechanisms of molecular oxygen activation. *Russ. Chem. Rev.* **76**, 988–1010 (2007).
29. Long, C. & Kearns, D. R. Selection rules for the intermolecular enhancement of spin forbidden transitions in molecular oxygen. *J. Chem. Phys.* **59**, 5729 (1973).
30. Hidemori, T., Akai, N., Kawai, A. & Shibuya, K. Intensity enhancement of weak $O_2a^1\Delta_g - X^3$ emission at 1270 nm by collisions with foreign gases. *J. Phys. Chem. A* **116**, 2032 (2012).
31. Janssen, J. Analyse spectrale des éléments de l'atmosphère terrestre. *C. R. Acad. Sci.* **101**, 649–651 (1885).
32. Janssen, J. Sur les spectres d'absorption de l'oxygène. *C. R. Acad. Sci.* **102**, 1352 (1886).
33. Tabisz, G. C., Allin, E. J. & Welsh, H. L. Interpretation of the visible and near-infrared absorption spectra of compressed oxygen as collision-induced electronic transitions. *Can. J. Phys.* **47**, 2859–2871 (1969).
34. Greenblatt, G. D., Orlando, J. J., Burkhoder, J. B. & Ravishankara, A. R. Absorption measurements of oxygen between 330 and 1140 nm. *J. Geophys. Res.* **95**, 18577–18582 (1990).
35. Sneep, M., Ityaksov, D., Aben, I., Linnartz, H. & Ubachs, W. Temperature-dependent cross sections of O_2–O_2 collision-induced absorption resonances at 477 and 577 nm. *J. Quant. Spectrosc. Radiat. Transf.* **98**, 405–424 (2006).
36. Thalman, R. & Volkamer, R. Temperature dependent absorption cross-sections of O_2–O_2 collision pairs between 340 and 630 nm and at atmospherically relevant pressure. *Phys. Chem. Chem. Phys.* **15**, 15371–15381 (2013).
37. Karman, T., van der Avoird, A. & Groenenboom, G. C. Potential energy and dipole moment surfaces of the triplet states of the $O_2(X^3\Sigma_g^-)$–$O_2(X^3\Sigma_g^-, a^1\Delta_g, b^1\Sigma_g^+)$ complex. *J. Chem. Phys.* **147**, 084306 (2017).
38. Karman, T., van der Avoird, A. & Groenenboom, G. C. Communication: multiple-property-based diabatization for open-shell van der Waals molecules. *J. Chem. Phys.* **144**, 121101 (2016).
39. Zagidullin, M. V., Pershin, A. A., Azyazov, V. N. & Mebel, A. M. Luminescence of the $(O_2(a^1\Delta_g))_2$ collisional complex in the temperature range of 90–315 K: experiment and theory. *J. Chem. Phys.* **143**, 244315 (2015).
40. Karman, T., van der Avoird, A. & Groenenboom, G. C. Line-shape theory of the $X^3\Sigma_g^- \rightarrow a^1\Delta_g$, $b^1\Sigma_g^+$ transitions in O_2–O_2 collision-induced absorption. *J. Chem. Phys.* **147**, 084307 (2017).
41. Richard, C. et al. New section of the HITRAN database: collision-induced absorption (CIA). *J. Quant. Spectrosc. Radiat. Transf.* **113**, 1276–1285 (2012).
42. Gordon, I. E. et al. The HITRAN2016 molecular spectroscopic database. *J. Quant. Spectrosc. Radiat. Transf.* **203**, 3–69 (2017).
43. Olver, F. W. J., Lozier, D. W., Boisvert, R. F. & Clark, C. W. *The NIST Handbook of Mathematical Functions* (Cambridge Univ. Press, Cambridge, 2010).
44. Nichols, R. Franck–Condon factors to high vibrational quantum numbers V: O_2 band systems. *J. Res. Nat. Bur. Stand. A* **69A**, 369–373 (1965).
45. Drouin, B. J. et al. Multispectrum analysis of the oxygen A-band. *J. Quant. Spectrosc. Radiat. Transf.* **186**, 118–138 (2017).
46. Karman, T., Miliordos, E., Hunt, K. L. C., Groenenboom, G. C. & van der Avoird, A. Quantum mechanical calculation of the collision-induced absorption spectra of N_2–N_2 with anisotropic interactions. *J. Chem. Phys.* **142**, 084306 (2015).
47. Buryak, I., Lokshtanov, S. & Vigasin, A. CCSD(T) potential energy and induced dipole surfaces for N_2–$H_2(D_2)$: retrieval of the collision-induced absorption integrated intensities in the regions of the fundamental and first overtone vibrational transitions. *J. Chem. Phys.* **137**, 114308 (2012).
48. Moraldi, M. & Frommhold, L. Collision-induced infrared absorption by H_2–He complexes: accounting for the anisotropy of the interaction. *Phys. Rev. A* **52**, 274 (1995).

Acknowledgements

This work was funded by the Netherlands Organisation for Scientific Research (NWO; grant 022.003.048). T.K. acknowledges additional support by the EU COST Action MOLIM (CM1405) and a pre-doctoral fellowship of the Smithsonian Astrophysical Observatory. A.B. and D.H.P. acknowledge EU H2020 ITN-EID project 'PUFF' (grant no. 642820) for support. I.E.G. is supported by NASA AURA program grant NNX14AI55G.

Author contributions

The theory was developed by T.K., A.v.d.A. and G.C.G. Cavity ring-down experiments were performed M.A.J.K., A.B., D.H.P. and W.J.v.d.Z. I.E.G. contributed to the comparison between experiment and theory.

Competing interests

The authors declare no competing interests.

Additional information

Supplementary information is available for this paper at https://doi.org/10.1038/s41557-018-0015-x.

Reprints and permissions information is available at www.nature.com/reprints.

Correspondence and requests for materials should be addressed to G.C.G.

Publisher's note: Springer Nature remains neutral with regard to jurisdictional claims in published maps and institutional affiliations.